doi:10.1093/brain/awp112 Brain 2009: 132; 1764–1782 | 1764

BRAIN
A JOURNAL OF NEUROLOGY

Dynamic changes of striatal and extrastriatal abnormalities in glutaric aciduria type I

Inga Harting,[1] Eva Neumaier-Probst,[2] Angelika Seitz,[1] Esther M. Maier,[3] Birgit Assmann,[4] Ivo Baric,[5] Monica Troncoso,[6] Chris Mühlhausen,[7] Johannes Zschocke,[8] Nikolas P. S. Boy,[9] Georg F. Hoffmann,[9] Sven F. Garbade[9,*] and Stefan Kölker[9,*]

1 Department of Neuroradiology, University of Heidelberg, Heidelberg, Germany
2 Department of Neuroradiology, University Hospital Mannheim of the University of Heidelberg, Mannheim, Germany
3 Department of Biochemical Genetics and Molecular Biology, Dr von Hauner Children's Hospital, Ludwig-Maximilians-University, Munich, Germany
4 Department of General Pediatrics, University Children's Hospital, Heinrich-Heine University, Düsseldorf, Germany
5 Department of Pediatrics, University Hospital Center, Zagreb, Croatia
6 Servicio Neurologico Infantil, Hospital Clinico San Borja Arriaran, Santiago, Chile
7 Department of Pediatrics, University Medical Center Hamburg-Eppendorf, Hamburg, Germany
8 Institute of Human Genetics and Clinical Genetics, Medical University of Innsbruck, Innsbruck, Austria
9 Department of General Pediatrics, Division of Inborn Metabolic Disease, University Children's Hospital, Heidelberg, Germany

*These authors contributed equally to this work.

Correspondence to: Dr Stefan Kölker,
Department of General Pediatrics,
Division of Inborn Metabolic Diseases,
University Children's Hospital Heidelberg,
Im Neuenheimer Feld 430,
D-69120 Heidelberg, Germany
E-mail: Stefan.Koelker@med.uni-heidelberg.de

In glutaric aciduria type I, an autosomal recessive disease of mitochondrial lysine, hydroxylysine and tryptophan catabolism, striatal lesions are characteristically induced by acute encephalopathic crises during a finite period of brain development (age 3–36 months). The frequency of striatal injury is significantly less in patients diagnosed as asymptomatic newborns by newborn screening. Most previous studies have focused on the onset and mechanism of striatal injury, whereas little is known about neuroradiological abnormalities in pre-symptomatically diagnosed patients and about dynamic changes of extrastriatal abnormalities. Thus, the major aim of the present retrospective study was to improve our understanding of striatal and extrastriatal abnormalities in affected individuals including those diagnosed by newborn screening. To this end, we systematically analysed magnetic resonance imagings (MRIs) in 38 patients with glutaric aciduria type I diagnosed before or after the manifestation of neurological symptoms. To identify brain regions that are susceptible to cerebral injury during acute encephalopathic crises, we compared the frequency of magnetic resonance abnormalities in patients with and without such crises. Major specific changes after encephalopathic crises were found in the putamen ($P < 0.001$), nucleus caudatus ($P < 0.001$), globus pallidus ($P = 0.012$) and ventricles ($P = 0.001$). Analysis of empirical cumulative distribution frequencies, however, demonstrated that isolated pallidal abnormalities did not significantly differ over time in both groups ($P = 0.544$) suggesting that isolated pallidal abnormalities are not induced by acute crises—in contrast to striatal abnormalities. The manifestation of motor disability was associated with signal abnormalities in putamen, caudate, pallidum and ventricles. In addition, we found a large number of extrastriatal abnormalities in patients with and without preceding encephalophatic crises. These abnormalities include widening

Received October 22, 2008. Revised March 7, 2009. Accepted March 26, 2009. Advance Access publication May 11, 2009

of anterior temporal and sylvian CSF spaces, pseudocysts, signal changes of substantia nigra, nucleus dentatus, thalamus, tractus tegmentalis centralis and supratentorial white matter as well as signs of delayed maturation (myelination and gyral pattern). In contrast to the striatum, extrastriatal abnormalities were variable and could regress or even normalize with time. This includes widening of sylvian fissures, delayed maturation, pallidal signal changes and pseudocysts. Based on these results, we hypothesize that neuroradiological abnormalities and neurological symptoms in glutaric aciduria type I can be explained by overlaying episodes of cerebral alterations including maturational delay of the brain *in utero*, acute striatal injury during a vulnerable period in infancy and chronic progressive changes that may continue lifelong. This may have widespread consequences for the pathophysiological understanding of this disease, long-term outcomes and therapeutic considerations.

Keywords: metabolism; striatum; maturation; neuroradiology; brain injury

Abbreviations: BSID-II = Bayley Scales of Infant Development, second edition; HAWIK-III = Hamburg Wechsler Intelligence Test for children, third edition; HAWIVA-III = Hannover Wechsler Intelligence Test for pre-school children, third edition; MR(I) = magnetic resonance (imaging); SON-R = Snijders-Oomen Non-verbal Intelligence Test, revised version.

Introduction

Glutaric aciduria type I is a rare cerebral organic aciduria caused by inherited deficiency of glutaryl-CoA dehydrogenase. The disease has an estimated prevalence of 1 in 100 000 newborns (Kölker *et al*., 2007*a*); more than 150 *GCDH* gene mutations are known (Goodman *et al*., 1998; Zschocke *et al*., 2000). Biochemically, accumulation of glutaric acid, 3-hydroxyglutaric acid and glutarylcarnitine is found. Two arbitrary biochemical subgroups, low and high excretors, have been described (Baric *et al*., 1999). Past studies, however, have not identified any correlation between the biochemical and clinical phenotype (Christensen *et al*., 2004; Kölker *et al*., 2006). Untreated, most patients develop an acute encephalopathic crisis during a finite period (age 3–36 months) of brain development resulting in acute striatal injury and, subsequently, dystonia (Kölker *et al*., 2006). Some patients may develop spasticity or akinetic-rigid parkinsonism in addition (Kyllerman *et al*., 2004; Gitiaux *et al*., 2008). A few patients have developed neurologic disease without encephalopathic crisis. These variants have been termed insidious-onset (Hoffmann *et al*., 1996) and late-onset type (Bähr *et al*., 2002), however, there is no accepted classification. In pre-symptomatically diagnosed children, the combination of a low-lysine diet and L-carnitine supplementation, with an intensified emergency treatment during intercurrent illness has significantly improved the outcome (Monavari and Naughten, 2000; Strauss *et al*., 2003; Kölker *et al*., 2007*a*). Consequently, newborn screening for glutaric aciduria type I has been implemented in some countries (Chace *et al*., 2003; Lindner *et al*., 2006; Bijarnia *et al*., 2008).

Neuroradiological studies have primarily focused on striatal abnormalities (Brismar and Ozand, 1995; Desai *et al*., 2003; Elster, 2004; Oguz *et al*., 2005; Strauss *et al*., 2007; Gitiaux *et al*., 2008), whereas lesions in other deep grey matter nuclei have been described only sporadically (Twomey *et al*., 2003). In addition, alterations of the frontotemporal CSF spaces have commonly been observed. They consist of enlarged anterior temporal CSF spaces, incomplete opercularization and widening of sylvian fissures and are variably described as temporal hypoplasia, frontotemporal atrophy or 'batwing' appearance. Notably, widening of sylvian fissures and frontotemporal atrophy are already present at the time of birth in preterm and term babies with glutaric aciduria type I and even during the last trimester of pregnancy (Forstner *et al*., 1999; Lin *et al*., 2002). Patients with late-onset neurologic disease predominantly present with white matter abnormalities (Külkens *et al*., 2005). However, little is known about magnetic resonance imaging (MRI) in pre-symptomatically diagnosed patients, about extrastriatal abnormalities and the implication of MRI changes for the neurological presentation.

Patients and Methods

Patient groups and evaluation of cranial MRIs

Metabolic centres which have contributed to previous clinical studies (Kölker *et al*., 2006, 2007*a*) provided digitalized cranial MRIs of study patients. Cranial MRIs were sent to the study centre (SK, SFG, GFH: University Children's Hospital, Heidelberg, Germany), and, subsequently, were evaluated independently by three neuroradiologists (IH, ENP and AS) using a standardized protocol (Supplementary Table 1). Brain maturation stage was assessed according to myelination and gyration time tables (Barkovich, 2000; Van der Knaap and Valk, 2005). Signal alterations were rated as white matter abnormality if (i) they did not correspond to the normal pattern of myelinated and unmyelinated structures of a younger child; and/or (ii) the signal changes were more prominent than the signal of as yet unmyelinated white matter. They were not rated as abnormal if they were restricted to the parieto-occipital white matter, since these might well correspond to the normal 'terminal zones of myelination'. Retrospective neuroradiological assessment was made without knowledge of the disease course, the mode of diagnosis, treatment or any other relevant clinical information that might have influenced objectivity.

Sixty-eight cranial MRI studies consisting of at least T_2- and T_1-weighted sequences were performed between the ages of 9 days and 66 years (median age: 15 months) in 38 patients (18 female, 20 male). The majority of these patients were neurologically asymptomatic at the time of MRI ($n = 21$ patients), while 17 patients underwent MRI after the onset of neurological symptoms. In acutely injured patients, MRI was performed at least 1 week after the acute onset of neurologic symptoms, i.e. the chronic stage according to a recent definition (Strauss *et al*., 2007). One pre-symptomatically diagnosed patient with a subsequent crisis was only imaged before, but not after this crisis.

Patient information

For all patients, detailed information on birth date, diagnosis, gender, mutation analysis and/or enzyme analysis, organic acid analysis, clinical presentation, anthropometrics and neurodevelopment were reported as described (Kölker *et al*., 2007a). Age-adapted maintenance and emergency treatment protocols of study patients were in agreement with a recently published guideline for glutaric aciduria type I (Kölker *et al*., 2007b); these protocols having been used by contributing metabolic centres from Germany and some other countries at least since 1993.

To estimate the severity of neurological disease, we determined the handicap score and the morbidity score as previously described (Kölker *et al*., 2006). In brief, the handicap score is based on the overall estimation of motor disability by caring physicians [0 = unaffected; 1 = mild (mild-motor dysfunction without disability in daily life); 2 = moderate (moderate dysfunction causing some but no limiting disability); 3 = severe (limiting disability with few motor skills left); and 4 = very severe (loss of motor skills except voluntary eye movements)]. Morbidity score adds one point each for loss of mobility, feeding problems, respiratory problems and seizures, ranging from 0 (asymptomatic) to 4 (multiple morbidity). The manifestation of dystonia (0 = no; 1 = yes) was also included in the analysis. In addition, standardized psychological tests [Bayley Scales of Infant Development, second edition (BSID-II); Snijders-Oomen Non-verbal Intelligence Test, revised version (SON-R); Hamburg Wechsler Intelligence Test for children, third edition, German version (HAWIK-III) and Hannover Wechsler Intelligence Test for pre-school children, third edition, German version (HAWIVA-III)] were performed in some patients.

Patients were anonymized by initials, birth date and gender, and double entries were excluded by these parameters. Data were only included if written informed consent was obtained from patients and/or parents. No patient declined inclusion into this study. Patients with unconfirmed diagnosis were excluded. The study was approved by the Institutional Ethics Committee of the University of Heidelberg (# 314/2002).

Statistical analysis

Statistical analysis was performed using R (R Development Core Team, 2008). To evaluate the frequency of MRI abnormalities in specific brain regions, we calculated the region-specific percentage of pathological changes. To estimate the impact of acute encephalopathic crises on MRI changes, we subdivided neuroradiological results for patients with and without reported crises. Region-specific differences between these groups were analysed using Fisher's exact test. To prevent bias by variant disease forms, we performed this analysis twice: once excluding the five patients with suggested variant disease forms (insidious-onset: $n = 1$; late onset: $n = 4$), and again including these patients in the group without encephalopathic crises.

With regard to the age dependence of specific MRI changes, differences in time points and frequency of MRI studies had to be taken into consideration. We calculated the empirical cumulative distribution function of age-dependent changes assuming that longitudinal changes in each patient are due to the same mechanism and that therapeutic effectiveness and adherence to treatment were the same for all study patients. Results of the MRI evaluation were used in a dichotomized way considering the presence or absence of MRI abnormalities but not their gradual intensity. Subsequently, differences of age-dependent MRI abnormalities between patients with and without acute encephalopathic crises were analysed using the Peto and Peto modifications of the Wilcoxon Gehan test for left-censored data (Harrington and Fleming, 1982; Helsel, 2005). Data were left-censored for MRI abnormalities, because brain abnormalities develop during a variable time before diagnosis by MRI. If more than one MRI of a single study patient was included, statistical analysis considered only the MRI, which first described a specific pathology.

To investigate the relation between MRI abnormalities and neurological signs, we used the Kruskal–Wallis test and subsequent Benjamini–Hochberg correction of *P*-values (Benjamini and Hochberg, 1995).

Results

Exemplified follow-up investigations of five patients without striatal injury

Case reports of four neonatally diagnosed children and of one child with suggested late-onset disease variant are presented prior to the analysis of study results. We hereby aim to highlight the variability of MRI abnormalities and neurological presentation in patients without acute striatal injury.

Case 1: Progressive extrastriatal abnormalities accompanied by mild-mental retardation

A macrocephalic boy of consanguineous Turkish parents born at term was diagnosed by newborn mass screening in Germany (Patient #25, Table 1). He is homozygous for E365K in the *GCDH* gene and has 1% residual enzyme activity. Treatment with low-lysine diet and carnitine was started at age 10 days, however, intermittent episodes of increased lysine intake and irregular carnitine supplementation were reported by his parents. These episodes were paralleled by transiently decreased plasma carnitine concentrations and increased urinary glutaric acid and 3-hydroxyglutaric acid concentrations (Supplementary Fig. 1A). During the first 2 years of life he was admitted to hospital five times for the initiation of emergency treatment. Encephalopathic crises were prevented, although twice the start of emergency treatment was delayed for >24 h. He has not developed a movement disorder and was able to sit independently at 6 months, to stand at 12 months and to walk at 15 months of age. He speaks German and Turkish fluently. Psychological testing revealed mild-mental retardation using BSID-II (mental developmental index at ages 12 and 26 months: 78 and 58) and SON-R (IQ at ages 47 and 55 months: 57 and 53, respectively).

Cranial MRI was performed at ages 5, 12 and 26 months. MRI revealed severe, symmetrical widening of anterior CSF spaces and sylvian fissures as well as progressive grey matter abnormalities, namely of globus pallidus, thalamus, dentate nucleus and very discretely of the substantia nigra. White matter involvement consisted of delayed myelination at 26 months and T_2 hyperintensity of periventricular and lobar white matter and central tegmental tracts (Fig. 1).

Table 1 Study population

Patient	Gender	Nation of origin	DOB (year)	Death (year)	Diagnosis (months)	Treatment (months)	MRI (months)	Genotype	Enzyme (%)	Excretor type	Crisis (months)	Disease course	Disability	Diet	Carnitine
A. Selective screening following acute encephalopathic crisis															
3	M	Chile	1997		18	18	19	Y113H/Y113H	ND	HE	14	Classic	Severe	PROT	+
5	M	Chile	2002		15	15	12	Y113H/Y113H	ND	HE	11	Classic	Moderate	LYS	+
6	F	Chile	1995		12	12	14	V133M/A385V	ND	ND	12	Classic	Moderate	PROT	+
13	F	Croatia	2004		6	6	5	R402W/R402W	0%	HE	4.5	Classic	Severe	LYS	+
17	M	Chile	1995	1999	12	12	13; 18	A293T/A293T	0%	HE	12; 46	Classic	Very severe	PROT	+
20	F	Chile	1993		12	12	18	R402W/R402W	0%	HE	12	Classic	Moderate	PROT	+
24	F	Germany	1984		37	37	258	A421V/A421V	0%	HE	37	Classic	Moderate	LYS	+
26	M	Chile	1997		10	12	11	Y113H/R402W	0%	HE	10	Classic	Mild	PROT	+
28	F	Turkey	2001		10	10	10; 20	M263W/M263W	29%	LE	10	Classic	Severe	LYS	+
30	M	NL	2002		27	27	27	ND	5%	LE	7	Classic	Mild	LYS	+
31	M	Chile	1989	2002	36	36	36	R161Q/R402W	0%	HE	8	Classic	Very severe	PROT	+
B. Selective screening following late-onset of neurological symptoms (i.e. without reported preceding crises)															
10	F	Germany	1976		352	352	352	ND	ND	HE	None	Late	None	PROT	+
12	M	Austria	1987		176	176	176	R88C/R88C	0%	HE	None	Late	None	PROT	+
16	M	Germany	1937		785	785	797	R383C/R383C	0%	HE	None	Late	Severe	PROT	+
38	F	Germany	1998		103	103	102; 114; 126	R128Q/E414K	1%	HE	None	Late	None	PROT	+
C. Selective screening due to macrocephaly															
22	M	Germany/Indonesia	1989		24	24	40; 167; 192; 216	C176R/C185A	1%	HE	None	Asympt.	None	LYS	+
32	M	Croatia	1997		0.75	1	54	R402W/A421V	0%	HE	None	Asympt.	None	LYS	+
35	M	Turkey	1997	2006	1	1	67	E365K/E365K	1%	HE	6	Classic	Very severe	LYS	+
D. High-risk screening of families with known index patients															
21	M	Germany/Indonesia	1992		1	1	0.5; 50; 131; 156; 180	C176R/G185A	0%	HE	None	Asympt.	None	LYS	+
14	M	Croatia	2002		28	28	29	R402W/R402W	0%	HE	None	Asympt.	None	LYS	+
36	F	Turkey	2002		0.25	0.5	1; 25	E365K/E365K	1%	HE	9	Classic	Moderate	LYS	+
E. Newborn screening															
1	M	Turkey	2001		0.25	0.5	0.5	R402W/R402W	0%	HE	1; 5	Classic	Mild	LYS	+
2	F	Italy	2003		0.25	0.5	0.5; 12; 25; 40; 50	P248L/P248L	1%	HE	None	Asympt.	None	LYS	+
4	M	Turkey	2001		0.5	0.75	16	R402W/R402W	0%	HE	None	Asympt.	None	LYS	+
7	F	Germany	2003		0.25	0.25	2	A421V/R257W	0%	HE	None	Asympt.	None	LYS	+
8	F	Morocco	2005		0.25	0.25	1	Y413X/Y413X	ND	HE	None	Asympt.	None	LYS	+
9	M	Turkey	2003		0.25	0.25	0.5; 0.75	R383C/R383C	ND	HE	None	Asympt.	None	LYS	+

(continued)

Table 1. Continued

Patient	Gender	Nation of origin	DOB (year)	Death (year)	Diagnosis (months)	Treatment (months)	MRI (months)	Genotype	Enzyme (%)	Excretor type	Crisis (months)	Disease course	Disability	Diet	Carnitine
11	M	Germany	2003		0.25	0.25	2	S255W/S255W	6%	LE	None	Asympt.	None	LYS	+
15	M	Turkey	2002		0.25	0.25	1; 25	T180A/T180A	ND	HE	None	Asympt.	None	LYS	+
18	F	Germany	2003		0.25	0.5	0.5	ND	0.5%	HE	None	Asympt.	None	LYS	+
19	F	Germany	2004		0.25	0.25	1	R161Q/C228R	25%	LE	None	Asympt.	None	LYS	+
23	F	Romania	2003		0.25	0.25	8; 14; 26; 37; 48	R161W/A421V	0%	HE	None	Asympt.	None	LYS	+
25	M	Turkey	2002		0.25	0.5	5; 12; 26	E365K/E365K	1%	HE	None	Asympt.	None	LYS	+
27	F	Germany	2003		0.25	0.25	3	T214M/M388T	1%	HE	None	Asympt.	None	LYS	+
29	F	Germany	2001		0.25	4	9	Y155H/A421V	5%	LE	None	Asympt.	None	LYS	+
33	M	Germany	2005		0.25	0.25	0.5; 2	ND	ND	HE	None	Asympt.	None	LYS	+
34	F	Germany	1998		0.5	7	7; 12	A421V/R128Q	0%	HE	None	Insidious	Mild	LYS	+
37	M	Germany	2004		0.25	0.25	0.5; 6; 13; 25; 36	R313W/nf	1%	HE	None	Asympt.	None	LYS	+

Asympt. = neurologically asymptomatic patient; Classic = classic onset (i.e. acute encephalopathic crises); DOB = date of birth; Enzyme, GCDH enzyme analysis (percentage of residual activity); Excretor type = biochemical phenotype (according to the definition of Baric et al., 1999); F = female; Genotype; *GCDH* gene mutation analysis (protein code); HE = high excretor; Insidious; insidious-onset disease variant; Late = late-onset disease variant; LE = low excretor; LYS = lysine-restricted diet; M = male; ND = not determined; nf = no mutation found; NL = The Netherlands; Nation of origin, ethnic origin of parents; PROT = protein-restricted diet.

Case 2: Frontotemporal hypoplasia, pallidal T_2 hyperintensity and white matter abnormalities accompanied by normal development

A girl of consanguinous Italian parents born at term was diagnosed by newborn screening (Patient #2). Diagnosis was confirmed by mutation analysis (homozygosity for S248L) and enzyme analysis (1% residual activity). Treatment with low-lysine diet and carnitine was started at age 8 days. During the first 2 years of life she was admitted to hospital five times for emergency treatment. She reached gross motor milestones on time (sitting: 6 months, standing: 13 months, walking: 17 months). Psychological testing confirmed normal motor and mental development using BSID-II (mental developmental index at ages 12, 25 and 40 months: 103, 92 and 94), SON-R (IQ at age 43 months: 105) and HAWIVA-III (IQ at age 59 months: 104). She is now 5 years of age and speaks Italian and German fluently, and has not developed a movement disorder. Biochemical follow-up investigations suggest good adherence to therapy (Supplementary Fig. 1B).

Serial MRI was obtained at ages 0.5, 12, 25, 40 and 50 months. They document normalization of initially widened anterior temporal CSF spaces and sylvian fissures, completion of earlier delayed myelination, slow evolution of white matter abnormalities and significant regression of the initial pallidal T_2 hyperintensity (Fig. 2 and Supplementary Fig. 2).

Case 3: Resolution of frontotemporal hypoplasia and pseudocysts

A boy of non-consanguinous German parents born at term was diagnosed by newborn screening (Patient #37). Molecular genetics revealed only a single mutation at one allele (R313W) but enzyme analysis confirmed the diagnosis (1% residual enzyme activity). Treatment was started on postnatal Day 8. During the first 2 years of life, he was admitted to hospital for emergency treatment once. His motor development was normal (sitting: 6 months, standing: 11 months, walking: 16 months). Psychological testing confirmed normal motor and mental development (BSID-II: mental developmental index at ages 13 and 24 months: 97 and 90; HAWIVA-III: IQ at age 47 months: 95). He is now 4 years of age and speaks German fluently. To our knowledge, he has never developed secondary carnitine depletion. Urinary excretion of glutaric acid and 3-hydroxyglutaric acid has remained low during treatment (Supplementary Fig. 1C).

Serial MRI was performed at ages 0.5, 6, 13, 25 and 36 months. The initial examination revealed an immature pattern of gyration and myelination, normally observed at 34–35 weeks postconceptional age, in combination with subependymal pseudocysts and wide anterior temporal and sylvian CSF spaces. The follow-up scans document retarded, but ultimately completed myelination, resolution of subependymal pseudocysts and normalization of CSF spaces. These serial MRI images highlight that extrastriatal abnormalities may regress in patients with glutaric aciduria type I (Fig. 3).

Case 4: Evolving white matter abnormalities, cortical and cerebellar atrophy

A macrocephalic boy of non-consanguinous German and Indonesian parents born at term was diagnosed with glutaric

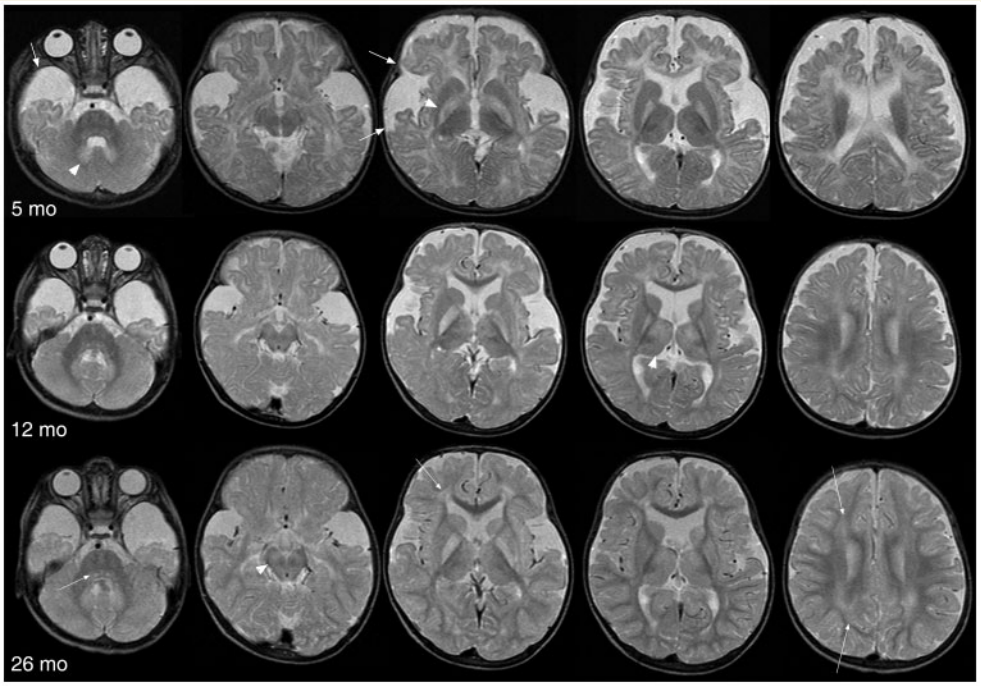

Figure 1 Sequential MRIs of Case 1 (i.e. Patient #25 according to Table 1) aged 5, 12 and 26 months (T_2-weighted images). This patient presents with the characteristic aspect of frontotemporal hypoplasia: widening of anterior temporal and sylvian CSF spaces (unilateral short arrows). Deep grey matter involvement is atypical with T_2 hyperintensity initially of pallidum and dentate nucleus, subsequently also of thalamus and very discretely of the substantia nigra (unilateral arrowheads). With time the striatal signal increases, however, not exceeding that of cortex. With ongoing, though at 26 months as yet incomplete myelination of the anterior temporal and frontobasal subcortical white matter, symmetrical T_2 hyperintensity of the periventricular and lobar white matter and of the central tegmental tracts becomes more prominent (unilateral arrows).

aciduria type I as a newborn by high-risk family screening (Patient #21). He is compound heterozygous for G185A and C176R resulting in complete loss of enzyme activity. This patient was admitted to hospital at 14 days of age and started on a low-lysine diet and carnitine supplementation. However, intermittently increased lysine intake and irregular carnitine supplementation were reported by his parents. In analogy to Case 1, transiently decreased carnitine levels and massive urinary excretion of glutaric and 3-hydroxyglutaric acid were found during these episodes (Supplementary Fig. 1D). He was never admitted to hospital for emergency treatment, and has not developed a movement disorder. He sat at 8 months, stood at 11 months and walked at 13 months of age. He is now 15 years of age and has passed the ninth class of general school (German secondary school). Psychological testing with HAWIK-III showed an average IQ (IQ at ages 13 and 15 years: 87 and 106).

Cranial MRI was performed at ages 0.5, 50, 131, 156 and 180 months. MRI findings consisted of the characteristically wide anterior temporal and sylvian CSF spaces and of atrophy, most pronounced in the cerebellum. Follow-up studies revealed evolving, confluent white matter abnormalities with involvement of the median corpus callosum (Fig. 4).

Case 5: Late-onset disease with extensive white matter abnormalities

A girl of non-consanguinous German parents was born at term and showed a normal development except for a transient motor delay (Patient #38). Despite several immunizations and febrile infectious diseases, she did not develop an acute encephalopathic crisis. She disliked protein-rich dairy products. At age 8.5 years, she became symptomatic with an episode of non-febrile severe nausea, recurrent vomiting, cephalgia and mild ataxia. No evidence for an infectious disease was found. Cranial MRI revealed extensive white matter abnormalities. Metabolic tests excluded peroxisomal or lysosomal disorders but demonstrated elevated urinary excretion of glutaric acid and 3-hydroxyglutaric acid (2100 and 110 mmol/mol creatinine) and low concentration of free plasma carnitine (3 μmol/l). Diagnosis was confirmed by enzyme and mutation analysis showing compound heterozygosity for R128Q and E414K and 1% of residual glutaryl-CoA dehydrogenase activity.

After the start of treatment symptoms gradually improved. Biochemical follow-up investigations showed a normalization of free plasma carnitine concentrations (45–67 μmol/l) and a moderate decrease in urinary glutaric acid excretion (1000–1200 mmol/mol creatinine). Neurological findings returned to normal, in particular there is no evidence for dystonia or chorea. Neuropsychological evaluation with HAWIK-III showed an average IQ of 96. MRI was repeated after 1 year (Fig. 5) and after 2 years of treatment. Despite clinical and biochemical improvement, extensive white matter abnormalities with involvement of the corpus callosum, T_2 hyperintensity of the thalamus, the tectal plate and periaqueductal zone and the dentate nucleus remained unchanged.

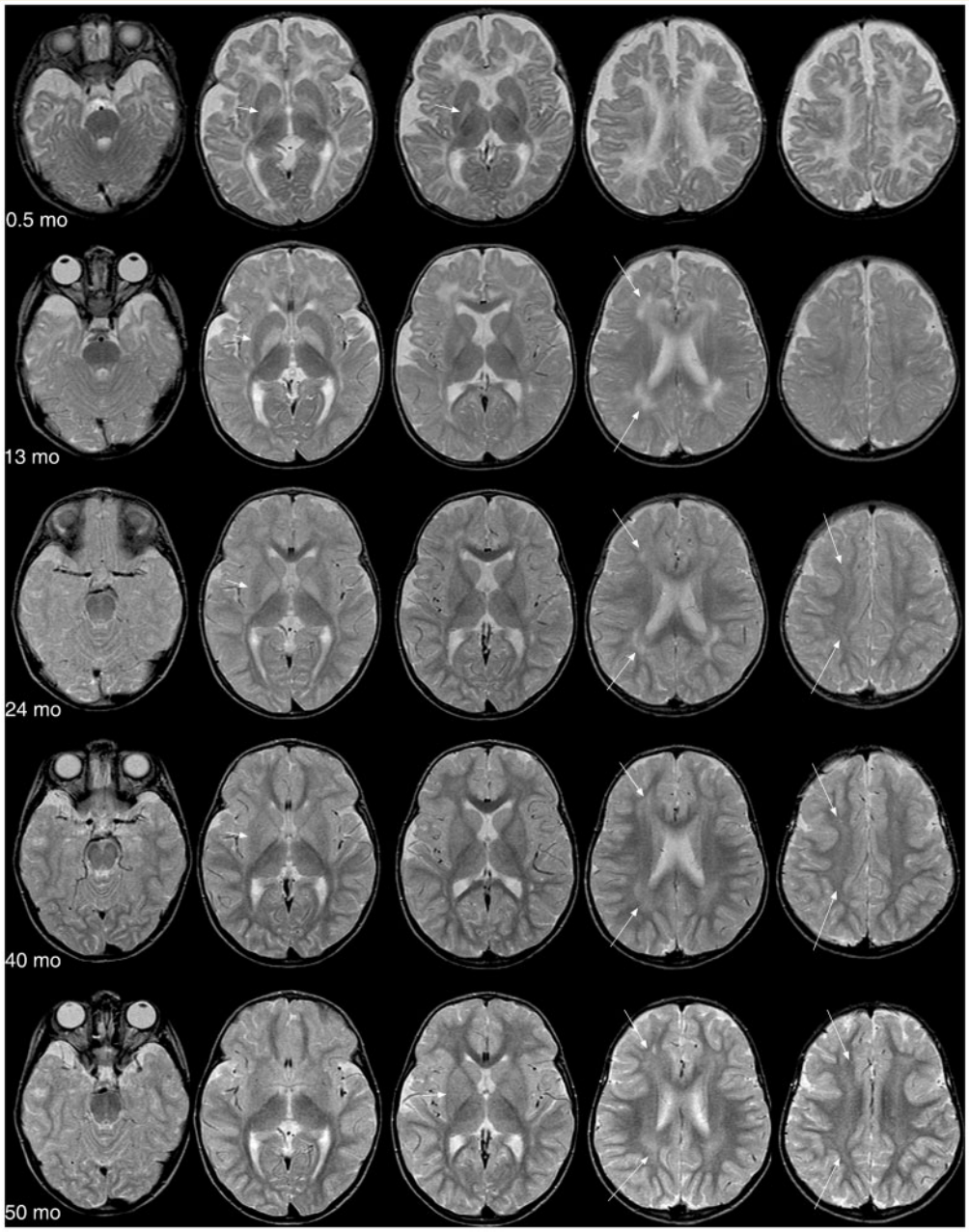

Figure 2 Sequential MRIs of Case 2 (Patient #2) between the ages of 0.5 and 50 months (T_2-weighted). With time the initially widened anterior temporal, sylvian and frontal CSF spaces normalize. The initial T_2 hyperintensity of the pallidum regresses; at 50 months pallidum and striatum are isointense and both slightly hypointense compared to cortex (unilateral short arrows). Myelination is delayed at 13 months [status of ~8 months, incomplete myelination on T_1 inversion recovery images (Supplementary Fig. 2)] and at 24 months (incomplete myelination of anterior temporal subcortical white matter), but progressing and ultimately complete. White matter abnormalities evolve from strongly hyperintense cap-like regions around frontal and dorsal horns to more diffuse, confluent signal of the periventricular and lobar white matter (unilateral long arrows).

Study population

The study included 68 cranial MRI scans from 38 patients (median age: 4.7 years, range: 1.4–69 years); basic information on study patients is summarized in Table 1. Eighteen patients were diagnosed by selective screening due to the manifestation of neurologic symptoms following acute encephalopathic crises ($n = 11$; median age at diagnosis: 13.5 months), late-onset of neurological symptoms during adolescence or adulthood without preceding crises ($n = 4$; age at diagnosis: 103, 176, 258 and 785 months), or the diagnostic work-up of macrocephaly in asymptomatic patients ($n = 3$; age at diagnosis: 0.75, 1 and 24 months). Three patients were diagnosed by high-risk screening of families with a previously identified index case

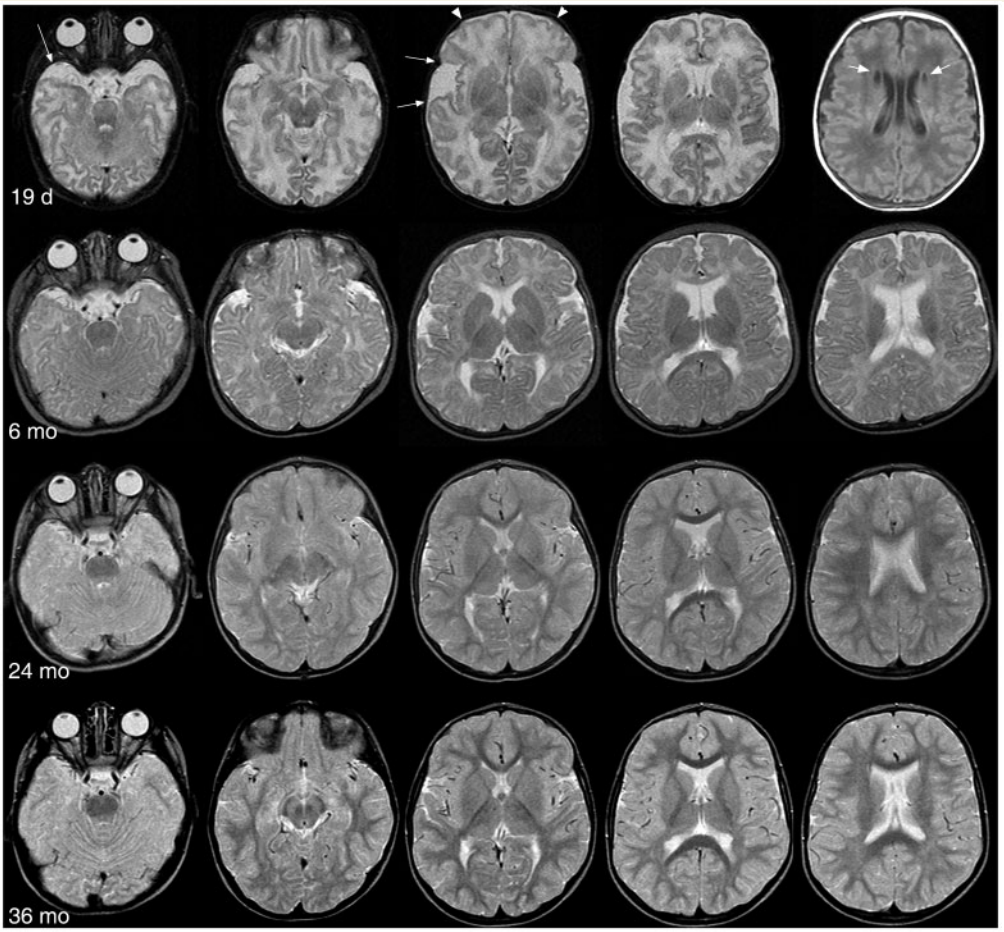

Figure 3 Sequential MRIs of Case 3 (Patient #37) between the ages of 19 days and 36 months (T_2-weighted images, except for fluid attenuated inversion recovery images, right upper corner). MRIs document normalization of frontotemporal hypoplasia (unilateral long arrows) and disappearance of subependymal pseudocysts (short arrows) and cavum vergae. The term newborn has an immature pattern of gyration and myelination normally observed at 34–35 weeks postconceptional age with too shallow and less branched sulci (arrowheads) and slightly, diffusely T_2 hyperintense white matter. The adult gyral pattern is normally reached by 3 months, and on follow-up MRI gyration is adequate for age. Myelination at 24 months is still insufficient in the subcortical temporal and frontal white matter, but at 36 months myelination is complete and the MRI is now normal.

(age at diagnosis: 0.25, 1 and 28 months), while 17 patients were identified by newborn screening (median age at diagnosis: 0.25 months). The majority of patients (86%) showed a high-excreting biochemical phenotype with R402W (19% of alleles), A421V (10%) and E365K (9%) as the most frequent mutations.

All patients who were diagnosed after the manifestation of acute encephalopathic crises (11/11) presented with dystonia and motor disability (mild: 2/11 patients, moderate: 4/11 patients, severe: 3/11 patients and very severe: 2/11 patients). In three patients with suggested late-onset variant, mild-neurological symptoms (ataxia, cephalgia and hand tremor) occurred transiently but resolved completely after the initiation of treatment, whereas neurological symptoms improved only slightly in the fourth Patient (#16). All three patients, who were diagnosed due to macrocephaly were neurologically asymptomatic at diagnosis. One patient (#35) developed dystonia after delayed start of emergency treatment during gastroenteritis.

All patients identified by newborn screening ($n = 17$) or high-risk family screening ($n = 3$) were asymptomatic at diagnosis and the majority of them remained asymptomatic (17/20 patients). One of them (#34), in whom start of maintenance treatment was delayed for 7 months, developed mild dystonia without apparent crises (insidious-onset). Two pre-symptomatically diagnosed children (#1 and #36) suffered an encephalopathic crisis during gastroenteritis due to inadequate emergency treatment.

Spectrum of MRI abnormalities

Wide anterior temporal and sylvian CSF spaces was the most common MRI abnormality (37/38 patients) and was found in all Patients (8/8) who were examined in the newborn period. The extent varied between discrete widening due to underdevelopment of the inferior frontal gyrus, which could only be adequately appreciated on sagittal images (Fig. 6), and massive widening easily observed on standard axial images. As hypoplasia of the inferior

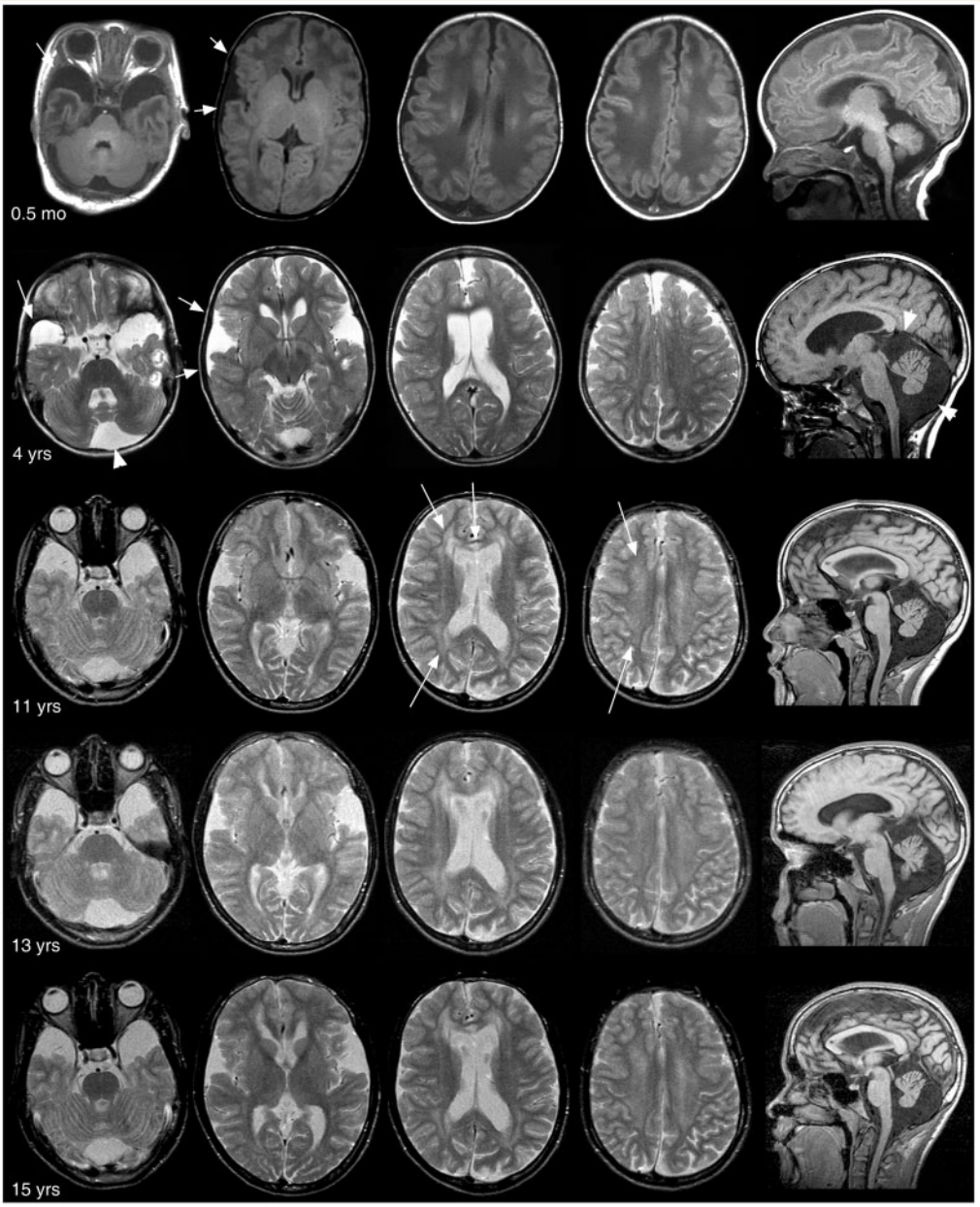

Figure 4 Serial MRIs of Case 4 (Patient #21) at 0.5 months (T_1-weighted, except for fluid attenuated inversion recovery images second from left), and at 4, 11, 13 and 15 years of age (axial T_2-weighted, sagittal T_1-weighted). Frontotemporal hypoplasia (unilateral short arrows) does not resolve in this patient. There is atrophy, most pronounced in the cerebellum, and in addition, enlargement of the supravermian cistern and the cisterna magna (arrowheads). Between the ages of 4 and 11 years white matter abnormalities develop with strongly T_2 hyperintense changes of the median genu corporis callosi and the periventricular white matter and with less pronounced, diffuse hyperintensity of the supratentorial white matter (unilateral long arrows).

frontal gyrus was visible in all patients with sagittal images covering insula and opercula, it seems likely that the frontal lobe was always involved. We therefore, use the term frontotemporal hypoplasia. Interestingly, the initial widening of CSF spaces diminished (Figs 1 and 2) or even normalized (Fig. 3). The frontotemporal and insular changes were similar to normal prenatal stages of frontotemporal development and opercularization.

Additional deviations from maturational changes of the developing brain, namely immature gyral pattern and myelination delay, were also common. A pattern of shallow sulci and white matter signal usually observed by 34–35 weeks of gestational age (Figs 3 and 6) was observed in four of the eight neonatally examined patients. Myelination delay was found in 21 of 38 patients and was most common between 20 and 28 months of age. Myelination delay was already present in four of the eight neonatally imaged patients, and was also found in Cases 1–4 (Figs 1–4). Nevertheless, myelination was complete by the age of 4 years—except for one Patient (#35).

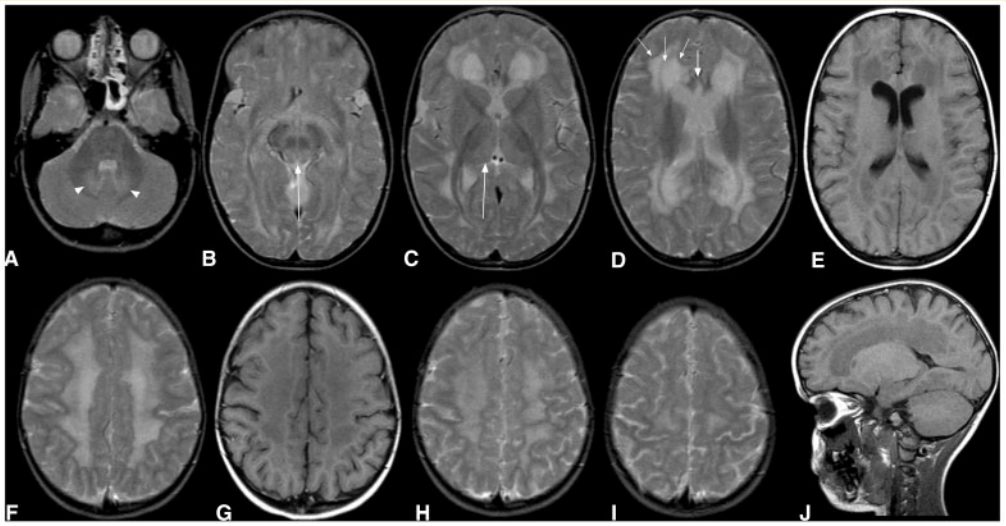

Figure 5 Follow-up MRI (**A–D**, **F**, **H** and **I**: T_2-weighted; **E**, **G** and **J**: T_1-weighted) of Case 5 (Patient #38) at the age of 9.5 years (i.e. 1 year after the diagnosis has been made and treatment has been started) demonstrates extensive white matter abnormalities persisting in the face of clinical and biochemical improvement since the initial MRI at age 8.5 years (not shown). As in Case 4 (Fig. 4), T_2 hyperintensity is 'bimodal': strongly T_2 hyperintense white matter separated by a rim of near normal signal from less hyperintense more peripheral white matter (unilateral thin arrows). Note involvement of the median corpus callosum (short arrow), of thalamus and midbrain (long arrows), and the dentate nuclei (arrowheads).

White matter signal abnormalities were also common (25/38 patients), the frequency increasing with age. They tended to be patchy or confluent in younger patients and were confluent in all patients examined after the age of 4 years. The periventricular white matter was involved in all patients and the signal alterations commonly extended into the deep white matter. Subcortical white matter was involved in seven patients, and corpus callosum in three patients. In the brainstem, abnormal, symmetrical T_2 hyperintensity of the central tegmental tracts was present in 14 patients.

Bilateral striatal abnormalities were found in 16 of 38 patients. Of note, none of the neonates had striatal changes inspite of one patient having already suffered from an encephalopathic crisis during the first week of life. Unexpectedly, abnormal signal of the pallidum was frequent, being present in 19 patients. Twelve patients presented with pallidal and striatal abnormalities, whereas seven patients had isolated pallidal changes. Other deep grey matter structures (Fig. 6) were much less often affected: the substantia nigra and dentate nuclei in seven patients and the thalamus in four patients.

Examples of striatal and extrastriatal MRI abnormalities are shown in Fig. 6.

MRI abnormalities following acute encephalopathic crises

To identify brain regions that are particularly susceptible to cerebral injury during acute encephalopathic crises, we compared the frequency of specific MRI abnormalities between patients with and without crises using Fisher's exact test (Table 2). In analogy to previous studies (Brismar and Ozand, 1995; Strauss *et al*., 2007), major changes after these crises were found in the basal ganglia, particularly affecting putamen and caudate (i.e. striatum), and less frequently the pallidum. Atrophy of affected basal ganglia structures resulted in the dilation of ventricles. Striatal abnormalities were also found in one patient with suggested insidious-onset variant, but not in four patients with late-onset type.

It is noteworthy that pallidal abnormalities were not only commonly found in combination with striatal abnormalities in dystonic patients with encephalopathic crises, but also as isolated findings in asymptomatic patients without encephalopathic crises (7/25 patients). In contrast to basal ganglia, the frequency of MRI changes in other brain regions did not differ between patients with and without encephalopathic crises—except for dilation of frontal CSF spaces, which showed a tendency to significance (Table 2).

Age-dependent changes of MR abnormalities

To identify age-dependent abnormalities and to distinguish them from acute pathologic changes induced by acute encephalopathic crises, we calculated empirical cumulative distribution functions of defined brain regions in patients with and without known encephalopathic crises. Assuming that specific MRI abnormalities are due to the same underlying mechanism in different patients, this statistical analysis allowed us to estimate longitudinal changes in patient subgroups although timing and frequency of MRIs differed between individual study patients. In contrast to

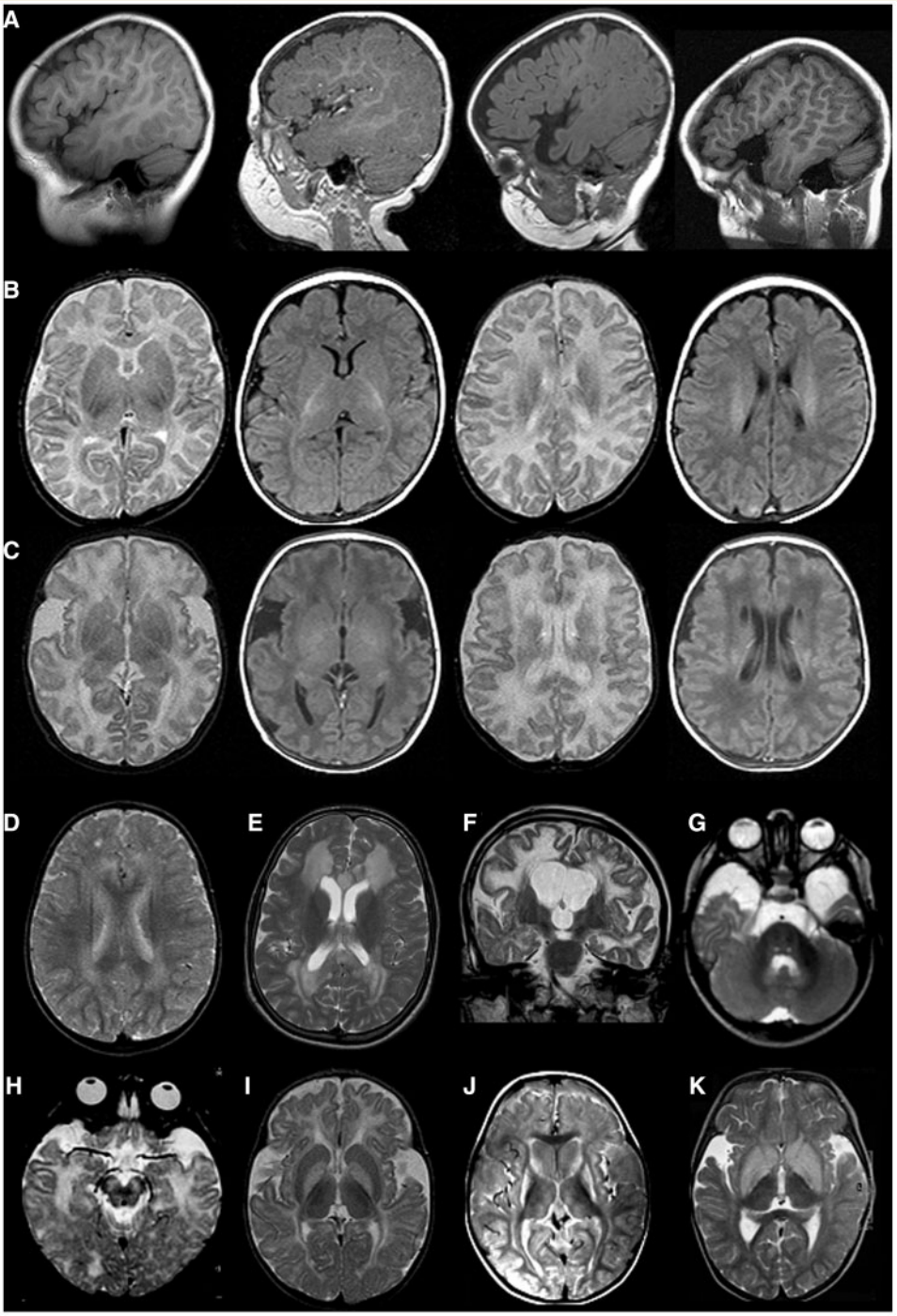

Figure 6 Examples of maturational (**A** and **C**), white matter (**C–G**) and grey matter (**G–K**) abnormalities in patients with glutaric aciduria type I. (**A**) Frontotemporal hypoplasia: the mild end of the spectrum of frontotemporal hypoplasia with discrete to clear (from left to right) underdevelopment of the inferior frontal gyrus, in more pronounced cases with accompanying hypoplasia of the superior temporal gyrus. (**B** and **C**) Delayed maturation: normal neonatal maturational stage (**B**) and immature gyral pattern and myelination delay in a 19-day-old neonate with glutaric aciduria type I (**C**; Patient #37). Sulci are more shallow and less branched in (**C**) than in (**B**). The white matter is slightly more T_2 hyperintense (first and third image from left) and T_1 hypointense (second and fourth image from left; arrows), respectively, and the contrast between white matter and cortical grey matter is greater than in (**B**). The normal T_1 hyperintense signal of the posterior limb of the internal capsule (**B**; short arrow) is missing (**C**). Additional findings in this neonate are wide sylvian CSF spaces, a cavum vergae and subependymal pseudocysts. (**D–G**) Examples of white matter signal abnormalities: predominantly periventricular white matter abnormalities (**D**; Patient #23), with a 'bimodal' pattern and involvement of the corpus callosum (**E**; Patient #10), and with extensive, asymmetrical changes involving the subcortical white matter (**F**; Case #16) and the central tegmental tracts (**G**; Patient #17). (**G–K**) Examples of grey matter changes: T_2 hyperintensity of the dentate nuclei (**G**; Patient #17) and the substantia nigra (**H**; Patient #26); isolated pallidal hyperintensity (**I**; Patient #23); involvement of thalamus in conjunction with atrophy and T_2 hyperintensity of putamen, caudate and pallidum 6 months after an encephalopathic crisis (**J**; Patient #17); swelling and T_2 hyperintensity of putamen, caudate and pallidum 14 days after an encephalopathic crisis (**K**; Patient #5).

Table 2 Region-specific frequency of MRI abnormalities

Region-specific MRI abnormalities	With AEC ($n=13$) (Percentage of patients)	w/o AEC ($n=19$) (Percentage of patients)	Odds ratio (95% CI)	*P*
1. Frontotemporal hypoplasia, dilated CSF spaces, subdural effusions				
Frontotemporal hypoplasia	100	90	Inf (0.13–Inf)	0.502
Dilated ventricles	77	16	15.7 (2.4–153)	**0.001**
Dilated external CSF spaces (frontal)	85	47	5.8 (0.89–67–8)	0.062
Dilated external CSF spaces (temporal)	100	90	Inf (0.13–Inf)	0.502
Dilated external CSF spaces (parieto-occipital)	39	21	2.3 (0.37–15.2)	0.427
Dilated external CSF spaces (interhemispheric)	54	37	2.0 (0.38–10.6)	0.473
Subdural effusions	0	0		
2. Deep grey matter structures				
Putamen	100	0	Inf (29.5–Inf)	**<0.001**
Caudate	92	11	76.0 (6.6–4414)	**<0.001**
Pallidum	85	53	8.7 (1.3–104)	**0.012**
Substantia nigra	25	16	1.7 (0.19–16.0)	0.653
Dentate nuclei	15	11	1.5 (0.1–6.24.0)	1
Thalamus	8	5	1.5 (0.02–124)	1
3. White matter				
Myelination delay	75	47	3.2 (0.56–24.3)	0.158
White matter disease	77	53	2.9 (0.51–21.7)	0.267
4. Infratentorial structures				
Cerebellum	0	16	0 (0–3.5)	0.253
Tractus tegmentalis centralis	50	28	2.5 (0.44–15.6)	0.266
5. Additional findings				
Cavum vergae	8	21	0.3 (0.01–3.9)	0.625

Calculations of odds ratios and *P*-values were performed using Fisher's exact test (patients with versus w/o acute encephalopathic crises, AEC). Calculations were based on majority decisions of all three raters for individual patients and cranial MRI scans. Significant differences are highlighted using bold letters. Five patients with suggested alternative disease variants (one patient with insidious-onset; four patients with late-onset) were excluded from this analysis. However, an inclusion of these patients to group 'w/o AEC' showed similar results (data not shown). In addition, one patient with acute crisis was excluded in whom cranial MRI was performed before crisis only.
AEC = acute encephalopathic crisis; CI = confidence interval; Inf = infinity.

Fisher's exact test, which analyses differences in frequencies of MRI abnormalities (Table 2), Peto and Peto test analyses differences in the time course of these MRI abnormalities among patients with and without encephalopathic crises. Peto and Peto test showed that striatal (putamen, caudate) MRI abnormalities differed between patients with and without encephalopathic crises, with time (Table 3). In contrast, the time course of pallidal MRI abnormalities occurring did not differ significantly between these groups suggesting that isolated pallidal abnormalities are not coupled to the manifestation of acute encephalopathic crises—in contrast to striatal lesions. Of course, pallidal changes were observed in a large proportion, in combination with striatal changes in patients with encephalopathy (12/19). However, an even larger proportion of patients with pallidal changes had concomitant white matter disease (17/19). Pallidal changes without white matter abnormalities were only observed in the context of striatal injury due to encephalopathic crises. Similar to white matter signal abnormalities, the frequency of pallidal abnormalities increased with the patient's age (Fig. 7). The presence of pallidal changes correlated both with encephalopathy and white matter changes, possibly reflecting that the pallidum is a myelin-rich grey matter structure (Van der Knaap and Valk, 2005).

Exemplied empirical cumulative distribution functions for MR abnormalities of cortex, putamen, pallidum and white matter in patients with and without acute encephalopathic crises are shown in Fig. 7.

Association of MRI abnormalities in the basal ganglia and motor dysfunction

Having identified MRI changes in neurologically asymptomatic and symptomatic patients, we sought to identify those MRI changes associated with motor disability. For this purpose, we compared individual MRI findings with the neurological outcome evaluating morbidity score, handicap score and dystonia at the same time MRIs were taken. Severe motor disability, indicated by a high-morbidity score and handicap score, and the onset of dystonia was associated with MRI abnormalities in putamen, caudate, pallidum and, consequently, with dilation of ventricles (Table 4, Fig. 8). In contrast, MRI abnormalities outside the basal ganglia were associated with a wide spectrum of neurological symptoms and thus did not allow an outline a clear-cut clinical phenotype. Only dilation of frontal CSF spaces showed a tendency to significance using handicap and morbidity score. As systematic testing of cognitive development was only performed in a subgroup of patients, the present study did not allow estimation of a graded quantitative impact of specific MRI abnormalities on cognitive dysfunction.

Table 3 Age-dependent MRI abnormalities

Brain regions	With versus without AEC
1. Frontotemporal hypoplasia, dilated CSF spaces, subdural effusions	
Frontotemporal hypoplasia	$\chi^2(1) = 1.2$, $P = 0.268$
Dilated ventricles	$\chi^2(1) = 1.1$, $P = 0.284$
Dilated external CSF spaces (frontal)	$\chi^2(1) = 1.3$, $P = 0.263$
Dilated external CSF spaces (temporal)	$\chi^2(1) = 1.2$, $P = 0.268$
Dilated external CSF spaces (parieto-occipital)	$\chi^2(1) = 0.1$, $P = 0.732$
Dilated external CSF spaces (interhemispheric)	$\chi^2(1) = 0.1$, $P = 0.703$
Subdural effusions	$\chi^2(1) = 0.5$, $P = 0.5$
2. Deep grey matter structures	
Putamen	**$\chi^2(1) = 7.9$, $P = 0.005$**
Caudate	**$\chi^2(1) = 4.4$, $P = 0.037$**
Pallidum	$\chi^2(1) = 0.4$, $P = 0.544$
Substantia nigra	$\chi^2(1) = 1.1$, $P = 0.299$
Dentate nuclei	$\chi^2(1) = 0.4$, $P = 0.544$
Thalamus	$\chi^2(1) = 1$, $P = 0.388$
3. White matter	
Myelination delay	$\chi^2(1) = 0$, $P = 0.882$
White matter disease	$\chi^2(1) = 0.3$, $P = 0.558$
4. Infratentorial structures	
Cerebellum	$\chi^2(1) = 1.5$, $P = 0.22$
Tractus tegmentalis centralis	$\chi^2(1) = 2.4$, $P = 0.122$
5. Additional findings	
Cavum vergae	$\chi^2(1) = 0.7$, $P = 0.392$

This table presents the Peto and Peto modification of the Wilcoxon Gehan test for left-censored data. Calculations were based on majority decisions of all three raters for individual patients and cranial MRI scans. Significant differences are highlighted using bold letters. Five patients with suggested alternative disease variants (one patient with insidious-onset; four patients with late-onset) were excluded from this analysis. However, an inclusion of these patients to group 'w/o AEC' showed similar results (data not shown). In addition, one patient with acute crisis was excluded in whom cranial MRI was performed before crisis only. AEC = acute encephalopathic crisis.

Discussion

The major results of the present retrospective study are that: (i) MRI abnormalities of patients with glutaric aciduria type I are more complex and dynamic than previously recognized; (ii) some MRI abnormalities are related to age and appear to manifest acutely or progressively following a distinct time pattern; (iii) some MRI alterations represent a maturational delay resolving with age rather than a brain injury and (iv) striatal, but not extra-striatal, abnormalities are associated with motor dysfunction.

The striatum—the classic lesion localization

Previous neuroradiological studies have primarily focused on acute striatal abnormalities following acute encephalopathic crises (Brismar and Ozand, 1995; Desai *et al*., 2003; Elster, 2004; Oguz *et al*., 2005; Strauss *et al*., 2007; Gitiaux *et al*., 2008). In combination with macrocephaly in infancy and abnormalities of the temporal and frontal lobes, acute striatal MRI abnormalities are highly suspicious for glutaric aciduria type I (Brismar and Ozand, 1995). On MRI, acute striatal abnormalities are most conspicuous on diffusion-weighted MRI and they are characterized by restricted diffusion and T_2 hyperintensity (Elster, 2004; Santos *et al*., 2005; Strauss *et al*., 2007). Recently, three stages of striatal injury were differentiated based on MRI changes, namely an acute stage with restricted diffusion presumably due to cytotoxic oedema, a subacute stage characterized by pseudo-normalization of apparent diffusion coefficient and swelling (vasogenic oedema) and a chronic atrophic stage with elevated apparent diffusion coefficient (Strauss *et al*., 2007). In their study, an unexpectedly large number of Patients (6/9) with striatal injury of undetermined onset despite diagnosis and start of treatment during the newborn period were classified as insidious-onset type (Strauss *et al*., 2007).

Our study confirms that signal changes of the striatum are the most specific MRI abnormalities arising in infants with acute onset of motor dysfunction. However, it does not confirm a high frequency of the insidious-onset variant. Almost all study patients with striatal abnormalities presented with acute motor symptoms during an episode likely to precipitate acute encephalopathic crises, e.g. gastroenteritis or pneumonia. The one exception was a presymptomatically diagnosed patient with insidious-onset of motor symptoms, in whom the initiation of treatment was delayed for 7 months. An apparent limitation of our study is the lack of diffusion-weighted imaging and, consequently, the inability to assess diffusion properties of lesions. The detection of striatal abnormalities is nevertheless not hampered by this: acutely injured patients were examined at least 7 days after the injury, at a time when signal changes are already conspicuous on T_2-weighted images. Moreover, all patients with insidious-onset of symptoms reported by Strauss *et al*. (2007) had not only elevated diffusion but also T_2 hyperintense lesions. In contrast, neither clinical signs of insidious-onset of striatal injury nor striatal T_2 hyperintensity and/or atrophy were found in our study patients in whom treatment was initiated immediately after the diagnosis of glutaric aciduria type I was suspected.

There is no generally accepted pathophysiological model for acute striatal injury in glutaric aciduria type I. Evidence is increasing that glutaric acid and 3-hydroxyglutaric acid heavily accumulate in the brain (Funk *et al*., 2005; Külkens *et al*., 2005; Sauer *et al*., 2006; Zinnanti *et al*., 2006; Keyser *et al*., 2008) inducing impairment of mitochondrial energy metabolism, and imbalance of excitatory and inhibitory neurotransmission (Kölker *et al*., 2004; Sauer *et al*., 2005; Stellmer *et al*., 2007; Zinnanti *et al*., 2007). These results favour a neurotoxicological model but cannot explain the age-dependent striatal vulnerability. To address this, various maturation-dependent aspects have been discussed including expression of glutamate and dopamine receptors, energy demand of the basal ganglia, cerebral lysine metabolism, myelination of the corticostriatal tracts, as well as unfavourable blood vessel geometry in the (lateral) striatum and high susceptibility of striatal medium spiny neurons (reviewed by Strauss and Morton, 2003; Zinnanti *et al*., 2007).

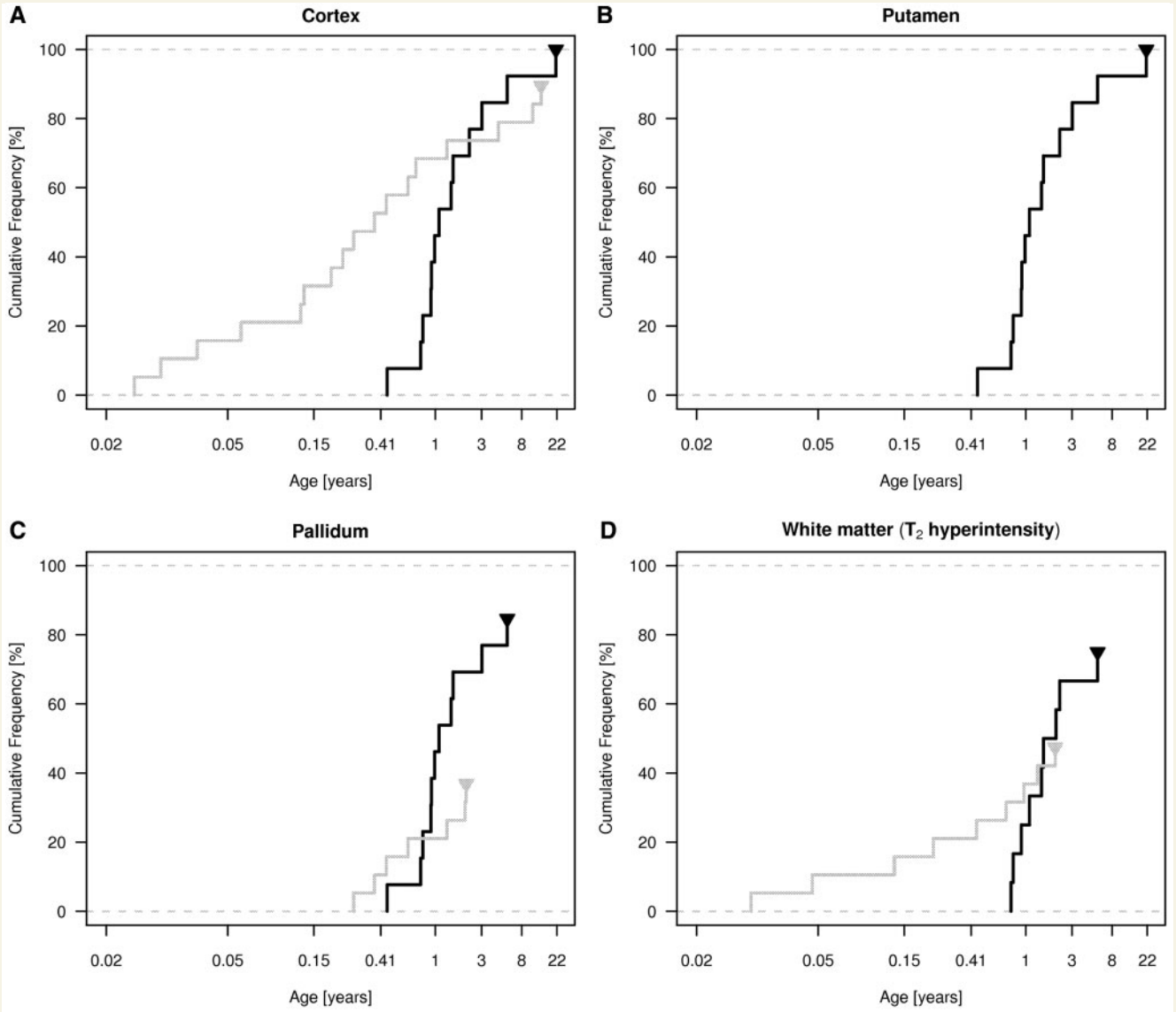

Figure 7 Empirical cumulative distribution function of exemplified brain regions. Empirical cumulative distribution function of abnormalities in different brain regions and their differences between patients with and without acute encephalopathic crises were calculated (Table 3) to evaluate the age dependence of MRI abnormalities. Results for frontotemporal hypoplasia (**A**) putamen (**B**), globus pallidus (**C**) and white matter T_2 hyperintensity (**D**) were shown. Grey lines, without encephalopathy; black lines, with encephalopathy. Note the logarithmic scale for age.

Beyond the striatum—the spectrum of MRI abnormalities in glutaric aciduria type I

In contrast to the striatum, abnormalities of other deep grey matter nuclei have been described only sporadically in glutaric aciduria type I. These include the demonstration of isolated pallidal MRI abnormalities in a few asymptomatic patients (Strauss *et al*., 2003; Twomey *et al*., 2003) as well as T_2 hyperintensity of other nuclei including substantia nigra and dentate nuclei (Twomey *et al*., 2003). For the present study, MRI was systematically evaluated for striatal and extrastriatal—grey and white matter—abnormalities. The results demonstrate that MRI abnormalities in extrastriatal brain regions are frequently found in patients with and without preceding encephalopathic crises.

Previously unreported, brain maturation was retarded in half of the neonatally imaged term babies with glutaric aciduria type I, their gyral pattern and white matter signal corresponding to that usually observed at 34–35 weeks postconceptional age. As the 'adult' gyral pattern is usually reached by 3 months of age, only the myelination stage is an indicator of brain maturation in older infants and children. Again, delayed myelination was a common finding in children with glutaric aciduria type I (59%). The progression and—depending on the age—completion of myelination observable in patients with sequential MRI and the completed myelination in all patients older than 4 years of age, except one,

Table 4 Association between MRI abnormalities and morbidity score

Brain regions	Rating[a]	*n*	Mean	SD	Median	Kruskal–Wallis test
1. Frontotemporal hypoplasia, dilated CSF spaces, subdurals effusions						
Frontotemporal hypoplasia	1	2	0	0	0	$\chi^2(1) = 1.8$, $P = 0.509$
	2	1	1	NA	1	
	3	33	0.70	0.92	0	
Dilated ventricles	1	22	0.23	0.53	0	**$\chi^2(1) = 14.3$, $P = 0.001$**
	2	9	1.22	0.97	1	
	3	5	1.6	0.89	2	
Dilated external CSF spaces (frontal)	1	15	0.33	0.62	0	$\chi^2(1) = 5.9$, $P = 0.082$
	2	17	0.71	0.85	0	
	3	4	1.75	1.26	2	
Dilated external CSF spaces (temporal)	1	2	0	0	0	$\chi^2(1) = 1.6$, $P = 0.448$
	2	14	0.57	0.76	0	
	3	20	0.80	1.01	0	
Dilated external CSF spaces (parieto-occipital)	1	25	0.63	0.92	0	$\chi^2(1) = 2.3$, $P = 0.318$
	2	10	0.5	0.71	0	
	3	1	2	NA	2	
Dilated external CSF spaces (interhemispheric)	1	20	0.63	0.96	0	$\chi^2(1) = 4.9$, $P = 0.173$
	2	14	0.43	0.65	0	
	3	2	2	0	2	
Subdural effusions	1	36	0.67	0.9	0	NA
	2	0	NA	NA	NA	
	3	0	NA	NA	NA	
2. Deep grey matter structures						
Putamen	1	22	0.18	0.5	0	**$\chi^2(1) = 21.2$, $P < 0.001$**
	2	4	0.75	0.96	0.5	
	3	10	1.7	0.67	2	
Caudate	1	22	0.23	0.53	0	**$\chi^2(1) = 19.2$, $P < 0.001$**
	2	6	0.67	0.82	0.5	
	3	8	1.88	0.64	2	
Pallidum	1	17	0.24	0.56	0	**$\chi^2(1) = 14.7$, $P = 0.002$**
	2	10	0.5	0.71	0	
	3	9	1.67	0.87	2	
Substantia nigra	1	30	0.74	0.94	0	$\chi^2(1) = 0.3$, $P = 0.901$
	2	6	0.5	0.84	0	
	3	0	NA	NA	NA	
Dentate nuclei	1	30	0.7	0.92	0	$\chi^2(1) = 0.2$, $P = 0.873$
	2	6	0.5	0.84	0	
	3	0	NA	NA	NA	
Thalamus	1	34	0.71	0.91	0	$\chi^2(1) = 1.4$, $P = 0.808$
	2	2	0	0	0	
	3	0	NA	NA	NA	
3. White matter						
Myelination delay	1	16	0.4	0.74	0	$\chi^2(1) = 1.9$, $P = 0.428$
	2	20	0.8	0.95	0.5	
T_2 hyperintensity	1	13	0.38	0.65	0	$\chi^2(1) = 2.9$, $P = 0.382$
	2	9	0.55	0.88	0	
	3	14	1	1	1	
4. Infratentorial structures						
Cerebellum	1	32	0.69	0.9	0	$\chi^2(1) = 0.7$, $P = 0.716$
	2	1	0	NA	0	
	3	3	0.67	1.15	0	
Tractus tegmentalis centralis	1	25	0.65	0.93	0	$\chi^2(1) = 0.7$, $P = 0.518$
	2	11	0.91	0.94	1	
5. Additional findings						
Cavum vergae	1	30	0.73	0.91	0	$\chi^2(1) = 1.3$, $P = 0.251$
	2	6	0.33	0.82	0	

Statistical analysis was performed using Kruskal–Wallis test with Benjamini–Hochberg correction of *P*-values. Significant differences were highlighted using bold letters. Two patients with incomplete neuroscores were excluded. Using dystonia (0 = no, 1 = yes) or handicap score (0–4 pts) instead of morbidity score the same associations between MRI abnormalities and neurological disease were identified (data not shown). NA = not applicable. a Rating of MRI abnormalities was performed according to the previously defined evaluation protocol (Supplementary Table 1).

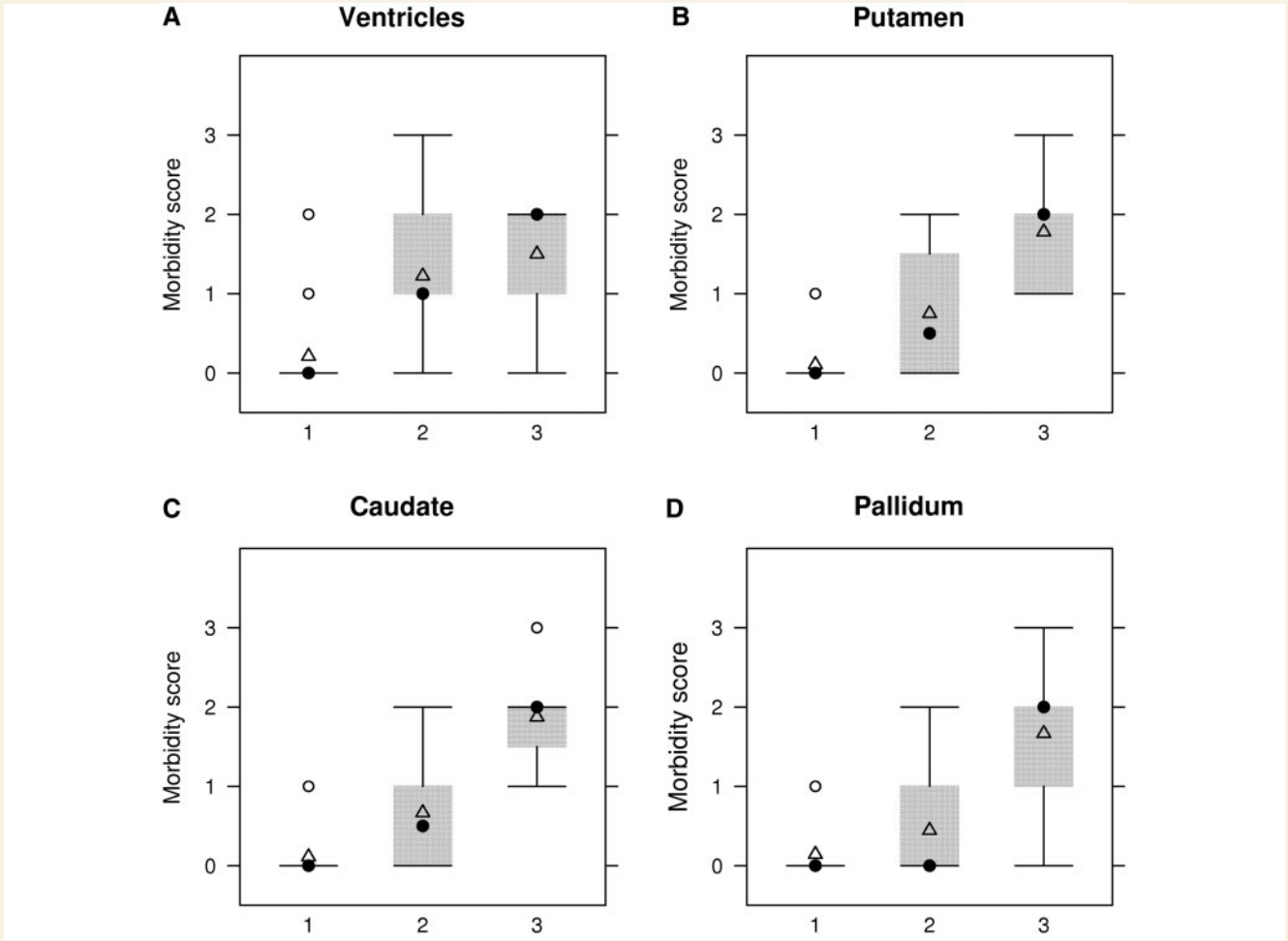

Figure 8 Association of MRI abnormalities in basal ganglia and motor dysfunction. Evaluation of motor disability using morbidity score (range: 0–4; 0 = asymptomatic; 4 = multiple morbidity) showed that the severity of motor disability was high in patients who had MRI abnormalities in dilated ventricles (**A**), putamen (**B**), caudate (**C**) and palladium (**D**). Using handicap score and manifestation of dystonia instead of morbidity score demonstrated the same associations to MRI abnormalities (not shown). A grey rectangle indicates the interquartile range, a filled circle the median and an open triangle the mean. Whiskers (black solid lines) extend 1.5 times from the first (25%) and third (75%) quantile, respectively. Outliers are marked by open circles.

suggest that though delayed, brain maturation is ultimately completed.

White matter abnormalities were common in both patient groups with (77%) and without (53%) encephalopathic crises, and did not correlate with encephalopathy, thereby suggesting that its development might not primarily depend on acute injury. White matter abnormalities were the major MRI finding in late-onset type. The neuropathological correlate of white matter abnormalities in glutaric aciduria type I is spongiform myelinopathy which seems to progress with age and has also been described in *Gcdh*-deficient mice (Chow *et al*., 1988; Soffer *et al*., 1992; Koeller *et al*., 2002; Kölker *et al*., 2003). Intramyelinic oedema with myelin vacuolation decreases extracellular space resulting in restricted diffusion. Conversely progressive damage and tissue loss and/or vasogenic oedema increase diffusion. The lack of diffusion-weighted images in this study, however, does not allow one to distinguish whether T_2 hyperintensity of white matter reflects intra- or extracellular water changes (Oguz *et al*., 2005; Strauss *et al*., 2007). Previous neuroradiological studies in glutaric aciduria type I patients have observed both restricted (Bähr *et al*., 2002; Oguz *et al*., 2005; Sonmez *et al*., 2007) and elevated diffusion (Strauss *et al*., 2007).

Of extrastriatal grey matter, the pallidum was the most commonly affected structure (51%), whereas substantia nigra (16%), dentate nuclei (11%) and thalamus (5%) were less frequently involved. Of note, pallidal abnormalities occurred in two patterns, either in combination with striatal changes following encephalopathy or as isolated lesions in patients without encephalopathy. Regardless of encephalopathic crises, the presence of pallidal abnormalities correlated with the presence of white matter abnormalities. Since the pallidum—and similarly thalamus and brainstem reticular formation—represents a myelin-rich grey matter structure, it seems likely that it will be affected by changes of both grey and white matter components (Kracun *et al*., 1984;

Van der Knaap and Valk, 2005). Pallidal MRI changes would result from acute grey matter injury during encephalopathic crises and/or from more slowly evolving, chronic white matter abnormalities and/or myelination delay. This is supported by the finding of a considerable decrease in myelin, but unaffected neuronal cell density of the globus pallidus in a post-mortem study (Chow *et al*., 1988). It further raises the question whether (transient) pallidal abnormalities in patients without encephalopathic crises possibly reflect delayed myelination instead of irreversible pallidal grey matter injury.

Time pattern of striatal and extrastriatal MRI abnormalities—from foetal life to adulthood

Four observations of the present study challenge our view on the neuropathogenesis of glutaric aciduria type I: (i) the high frequency of retarded brain maturation in neonates and infants; (ii) the regression of frontotemporal hypoplasia in pre-symptomatically diagnosed and treated patients; (iii) the completed myelination in virtually all children older than 4 years and (iv) the high frequency of white matter abnormalities increasing with age. These observations imply that in glutaric aciduria type I a chronically present, prenatally starting neurotoxicity may affect brain maturation as well as maintenance of white matter. This may be separate from the putative mechanism of acute striatal injury.

The hypothesis of glutaric aciduria type I prenatally affecting the brain is supported by the fact that widening of sylvian fissures and frontotemporal 'atrophy' are already present at the time of birth in preterm and term babies with glutaric aciduria type I and even during the last trimester of pregnancy (Forstner *et al*., 1999; Lin *et al*., 2002; Mellerio *et al*., 2008). In the present study, all neonatally imaged patients had widening of anterior temporal and sylvian CSF spaces and half of them had an immature gyral pattern and white matter signal. Comparing the appearance of the anterior temporal lobe and the sylvian fissure in our patients with the normal development observed on MRI, the pattern of abnormality in glutaric aciduria type I patients is similar to different stages of normal development. Gyration and opercularization occur latest in the frontal and temporal areas, namely those affected in glutaric aciduria type I (Van der Knaap *et al*., 1996; Garel, 2004). As regression of widened anterior temporal and sylvian CSF spaces occurred in neonatally diagnosed and treated patients, it seems likely that they presumably result from a potentially reversible (neurotoxic) arrest or delay of anterior temporal and opercular development.

With regard to putative pathomechanisms, it has been demonstrated that dicarboxylic acids such as glutaric acid and 3-hydroxyglutaric acid cannot easily permeate the blood–brain barrier (Hassel *et al*., 2002; Sauer *et al*., 2006). Intracerebral trapping of glutaric acid and 3-hydroxyglutaric acid is the biochemical prerequisite for subsequent cerebral injury (Sauer *et al*., 2006; Zinnanti *et al*., 2006; Keyser *et al*., 2008). This mechanism may become active as early as a functional blood–brain barrier is established already during foetal life. The expression of endothelial tight junctions and their adult-like distribution by midgestation suggest the establishment of a functional blood–brain barrier during the second half of fetal life (Virginto *et al*., 2004; Ballabh *et al*., 2005; Anstrom *et al*., 2007). This is a time-point when the major waves of neuronal migration have ceased, and neuronal differentiation and cortex lamination begins. Therefore, a functional blood–brain barrier may be important to guarantee a constant environment and protected habitat of the differentiating neurons (Virginto *et al*., 2004). Pathogenetically, we hypothesize that the establishment of a functional blood–brain barrier during the second half of pregnancy with consecutive accumulation of neurotoxic dicarboxylic acids in the brain compartment affects normal maturation in glutaric aciduria type I.

White matter changes in our patients consisted of myelination delay, which was already found in half of neonatally imaged patients, and of evolving T_2 hyperintensity of white matter. These were very often found in patients with and without acute crises and were statistically not linked with encephalopathic crises. Moreover, T_2 hyperintensity of white matter represents the characteristic MRI abnormality of late-onset disease (Bähr *et al*., 2002; Külkens *et al*., 2005). Whether this abnormality is induced during pre- or postnatal life (or both), is not yet known. Interestingly, immature oligodendroglial precursor cells can be injured by glutaric acid and 3-hydroxyglutaric acid (Gerstner *et al*., 2005). It is tempting to speculate that from the time of a functional blood–brain barrier onwards, neurotoxic dicarboxylic acids not only interfere with gyration and opercularization, but also with maturation of white matter (manifesting as myelination delay) and maintenance of white matter (manifesting as T_2 white matter signal abnormality).

In conclusion, the present study highlights that striatal and extrastriatal MRI abnormalities in glutaric aciduria type I are dynamic and complex. We suggest that chronic neurotoxicity affects brain maturation and myelin maintenance and that its manifestation may be separate from the mechanisms of acute injury due to encephalopathic crises. This may have widespread consequences for the establishment of a unifying pathophysiological model and for therapeutic considerations, e.g. whether dietary treatment should be performed lifelong. A certain limitation of this study, however, is its retrospective design and the inclusion of patients from different metabolic centres and birth cohorts, which may cause bias. Therefore, a prospective follow-up study is required to further investigate the formal and causal aspects of striatal and extrastriatal abnormalities, their clinical relevance and prevention.

Supplementary material

Supplementary material is available at *Brain* online.

Acknowledgements

We gratefully acknowledge the following colleagues for their kind contribution to this study: O. Bodamer (Vienna, Austria),

R. Ensenauer (Munich, Germany), T. de Koning (Utrecht, The Netherlands), S. Körner (Heidelberg, Germany), T. Meissner (Düsseldorf, Germany) and S. Sauer (Heidelberg, Germany).

Funding

German Federal Ministry of Education and Sciences (BMBF # 01GM0305); 'Kindness for Kids' Foundation, Munich, Germany (to S.K. and G.F.H.)

References

Anstrom JA, Thore CR, Moody DM, Brown WR. Immunolocalization of tight junction proteins in blood vessels in human germinal matrix and cortex. Histochem Cell Biochem 2007; 127: 205–13.

Bähr O, Mader I, Zschocke J, Dichgans J, Schulz JB. Adult onset glutaric aciduria type I presenting with a leukoencephalopathy. Neurology 2002; 59: 1802–4.

Ballabh P, Hu F, Kumarasiri M, Braun A, Nedergaard M. Development of tight junction molecules in blood vessels of germinal matrix, cerebral cortex, and white matter. Pediatr Res 2005; 58: 791–8.

Baric I, Wagner L, Feyh P, Liesert M, Buckel W, Hoffmann GF. Sensitivity and specificity of free and total glutaric and 3-hydroxyglutaric acid measurements of stable-isotope dilution assays for the diagnosis of glutaric aciduria type I. J Inherit Metab Dis 1999; 22: 867–81.

Barkovich AJ. Normal development of the neonatal and infant brain, skull, and spine. In: Barkovich AJ, editor. Pediatric neuroimaging. 3rd edn., Philadelphia: Lippincott Williams & Wilkins; 2000. p. 13–70.

Benjamini Y, Hochberg Y. Controlling the false discovery rate: a practical and powerful approach to multiple testing. J R Stat Soc Ser B Stat Method 1995; 57: 289–300.

Bijarnia S, Wiley V, Carpenter K, Christodoulou J, Ellaway CJ, Wilcken B. Glutaric aciduria type I: outcome following detection by newborn screening. J Inherit Metab Dis 2008; 31: 503–7.

Brismar J, Ozand PT. CT and MR of the brain in glutaric acidemia type I: a review of 59 published cases and a report of 5 new patients. Am J Neuroradiol 1995; 16: 675–83.

Chace DH, Kalas TA, Naylor EW. Use of tandem mass spectrometry for multianalyte screening of dried blood specimens from newborns. Clin Chem 2003; 49: 1797–817.

Chow CW, Haan EA, Goodman SI, Anderson RM, Evans WA, Kleinschmidt-DeMasters BK, et al. Neuropathology in glutaric acidemia type 1. Acta Neuropathol 1988; 76: 590–4.

Christensen E, Ribes A, Merinero B, Zschocke J. Correlation of genotype and phenotype in glutaryl-CoA dehydrogenase deficiency. J Inherit Metab Dis 2004; 27: 861–8.

Desai NK, Runge VM, Crisp DE, Crisp MB, Naul LG. Magnetic resonance imaging of the brain in glutaric acidemia type I: a review of the literature and a report of four new cases with attention to the basal ganglia and imaging technique. Invest Radiol 2003; 38: 489–96.

Elster AW. Glutaric aciduria type I: value of diffusion-weighted magnetic resonance imaging for diagnosing acute striatal necrosis. J Comput Assist Tomogr 2004; 28: 98–100.

Forstner R, Hoffmann GF, Gassner I, Heideman P, De Klerck JBC, Lawrenz-Wolf B, et al. Glutaric aciduria type I: ultrasonographic demonstration of early signs. Pediatr Radiol 1999; 29: 138–43.

Funk CBR, Prasad AN, Frosk P, Sauer S, Kölker S, Greenberg CR, et al. Neuropathological, biochemical, and molecular findings in a glutaric acidemia type 1 cohort. Brain 2005; 128: 711–22.

Garel C. Chapter 4: results. In: Garel C, editor. MRI of the fetal brain: normal development and cerebral pathologies. Berlin: Springer-Verlag; 2004. p. 35–114.

Gerstner B, Gratopp A, Marcinkowski M, Sifringer M, Obladen M, Buhrer C. Glutaric acid and its metabolites cause apoptosis in immature oligodendrocytes: a novel mechanism of white matter degeneration in glutaryl-CoA dehydrogenase deficiency. Pediatr Res 2005; 57: 771–6.

Gitiaux C, Roze E, Kinugawa K, Flamand-Rouvière C, Boddaert N, Apartis E, et al. Spectrum of movement disorders associated with glutaric aciduria type 1: a study of 16 patients. Mov Disord 2008; 23: 2392–7.

Goodman SI, Stein DE, Schlesinger S, Christensen E, Schwartz M, Greenberg CR, et al. Glutaryl-CoA dehydrogenase mutations in glutaric acidemia (type I): review and report of thirty novel mutations. Hum Mutat 1998; 00: 141–4.

Harrington DP, Fleming TR. A class of rank test procedures for censored survival data. Biometrika 1982; 69: 553–66.

Hassel B, Brathe A, Petersen D. Cerebral dicarboxylate transport and metabolism studied with isotopically labelled fumarate, malate and malonate. J Neurochem 2002; 82: 410–9.

Helsel DR. Nondetects and data analysis: statistics for censored environmental data. New York, USA: John Wiley & Sons; 2005.

Hoffmann GF, Athanassopoulos S, Burlina AB, Duran M, de Klerck JB, Lehnert W, et al. Clinical course, early diagnosis, treatment, and prevention of disease in glutaryl-CoA dehydrogenase deficiency. Neuropediatrics 1996; 27: 115–23.

Keyser B, Glatzel M, Stellmer F, Kortmann B, Lukacs Z, Kölker S, et al. Transport and distribution of 3-hydroxyglutaric acid before and during induced encephalopathic crises in a mouse model of glutaric aciduria type I. Biochim Biophys Acta 2008; 1782: 385–90.

Koeller DM, Woontner M, Crnic LS, Kleinschmidt-DeMasters B, Stephens J, Hunt EL, et al. Biochemical, pathologic and behavioural analysis of a mouse model of glutaric acidemia type I. Hum Mol Genet 2002; 11: 347–57.

Kölker S, Christensen E, Leonard JV, Greenberg CR, Burlina AB, Burlina AP, et al. Guideline for the diagnosis and management of glutaryl-CoA dehydrogenase deficiency (glutaric aciduria type I). J Inherit Metab Dis 2007b; 30: 5–22.

Kölker S, Garbade SF, Boy N, Maier EM, Meissner T, Mühlhausen C, et al. Decline of acute encephalopathic crises in children with glutaryl-CoA dehydrogenase deficiency identified by newborn screening in Germany. Pediatr Res 2007a; 62: 357–63.

Kölker S, Garbade SF, Greenberg CR, Leonard JV, Saudubray JM, Ribes A, et al. Natural history, outcome and therapeutic efficacy in children and adults with glutaryl-CoA dehydrogenase deficiency. Pediatr Res 2006; 59: 840–7.

Kölker S, Hoffmann GF, Schor DS, Feyh P, Wagner L, Jeffrey I, et al. Glutaryl-CoA dehydrogenase deficiency: region-specific analysis of organic acids and acylcarnitines in post mortem brain predicts vulnerability of the putamen. Neuropediatrics 2003; 34: 253–60.

Kölker S, Koeller DM, Okun JG, Hoffmann GF. Pathomechanisms of neurodegeneration in glutaryl-CoA dehydrogenase deficiency. Ann Neurol 2004; 55: 7–12.

Kracun I, Rösner H, Cosovic C, Stavljenic A. Topographical atlas of the gangliosides of the adult human brain. J Neurochem 1984; 43: 979–89.

Külkens S, Harting I, Sauer S, Zschocke J, Hoffmann GF, Gruber S, et al. Late-onset neurologic disease in glutaryl-CoA dehydrogenase deficiency. Neurology 2005; 64: 2142–4.

Kyllerman M, Skjeldal O, Christensen E, Hagberg G, Holme E, Lönnquist T, et al. Long-term follow-up, neurological outcome and survival rate in 28 Nordic patients with glutaric aciduria type1. Eur J Paediatr Neurol 2004; 8: 121–9.

Lin SK, Hsu SG, Ho ES, Tsai CR, Hseih YT, Lo FC, et al. Novel mutations and prenatal sonographic findings of glutaric aciduria (type I) in two Taiwanese families. Prenat Diagn 2002; 22: 725–9.

Lindner M, Ho S, Fang-Hoffmann J, Hoffmann GF, Kölker S. Neonatal screening for glutaric aciduria type I: strategies to proceed. J Inherit Metab Dis 2006; 29: 378–82.

Mellerio C, Marignier S, Roth P, Gaucherand P, des Portes V, Pracros JP, et al. Prenatal ultrasound and MRI findings in glutaric aciduria type 1: a de novo case. Ultrasound Obstet Gynecol 2008; 31: 712–4.

Monavari AA, Naughten ER. Prevention of cerebral palsy in glutaric aciduria type I by dietary management. Arch Dis Child 2000; 82: 67–70.

Oguz KK, Ozturk A, Cila A. Diffusion-weighted MR imaging and MR spectroscopy in glutaric aciduria type 1. Neuroradiology 2005; 47: 229–34.

R Development Core Team.R: a language and environment for statistical computing. Vienna: R foundation for statistical computing; 2008; http://www.R-project.org (last accessed: October 21, 2008).

Santos CC, Roach ES. Glutaric aciduria type I: a neuroimaging diagnosis? J Child Neurol 2005; 20: 588–90.

Sauer SW, Okun JG, Fricker G, Mahringer A, Crnic LR, Mühlhausen C, et al. Intracerebral accumulation of glutaric and 3-hydroxyglutaric acids in glutaryl-coenzyme A dehydrogenase deficiency, a biochemical risk factor for neurodegeneration. J Neurochem 2006; 97: 899–910.

Sauer SW, Okun JG, Schwab MA, Crnic LR, Hoffmann GF, Goodman SI, et al. Bioenergetics in glutaryl-coenzyme A dehydrogenase deficiency, a role for glutaryl-coenzyme A. J Biol Chem 2005; 280: 21830–6.

Sonmez G, Mutlu H, Ozturk E, Sildiroglu HO, Keskin AT, Basekim CC, et al. Magnetic resonance imaging findings of adult-onset glutaric aciduria type I. Acta Radiol 2007; 48: 557–9.

Soffer D, Amir N, Elpeleg ON, Gomori JM, Shalev RS, Gottschalk-Sabag S. Striatal degeneration and spongy myelinopathy in glutaric acidemia. J Neurol Sci 1992; 107: 199–204.

Stellmer F, Keyser B, Burckardt BC, Koepsell H, Streichert T, Glatzel M, et al. 3-Hydroxyglutaric acid is transported via the sodium-dependent dicarboxylate transporter NaDC3. J Mol Med 2007; 85: 763–70.

Strauss KA, Lazovic J, Wintermark M, Morton DH. Multimodal imaging of striatal degeneration in Amish patients with glutaryl-CoA dehydrogenase deficiency. Brain 2007; 130: 1905–20.

Strauss KA, Morton DH. Type I glutaric aciduria, part 2: a model of acute striatal necrosis. Am J Med Genet 2003; 121C: 53–70.

Strauss KA, Puffenberger EG, Robinson DL, Morton DH. Type I glutaric aciduria, part 1: natural history of 77 patients. Am J Med Genet 2003; 121C: 38–52.

Twomey EL, Naughten ER, Donoghue VB, Ryan S. Neuroimaging findings in glutaric aciduria type 1. Pediatr Radiol 2003; 33: 823–30.

Van der Knaap MS, Valk J, editors. Myelination and retarded myelination. Magnetic resonance of myelination and myelin disorders. 3rd edn., Berlin: Springer-Verlag; 2005. p. 37–65.

Van der Knaap MS, van Wezel-Meijler P, Barth PG, Barkhof F, Ader HJ, Valk J. Normal gyration and sulcation in preterm and term neonates: appearance on MR images. Radiology 1996; 200: 389–96.

Virginto D, Errede M, Robertson D, Capobianco C, Girolamo F, Vimercati A, et al. Immunolocalization of tight junction proteins in the adult and developing human brain. Histochem Cell Biol 2004; 122: 51–9.

Zinnanti WJ, Lazovic J, Housman C, LaNoue K, O'Callaghan JP, Simpson I, et al. Mechanism of age-dependent susceptibility and novel treatment strategy in glutaric acidemia type I. J Clin Invest 2007; 117: 3258–70.

Zinnanti WJ, Lazovic J, Wolpert EB, Antonetti DA, Smith MB, Connor JR, et al. A diet-induced mouse model for glutaric aciduria type I. Brain 2006; 129: 899–910.

Zschocke J, Quak E, Guldberg P, Hoffmann GF. Mutation analysis in glutaric aciduria type I. J Med Genet 2000; 37: 177–81.